Journal of
Science & Engineering
Volume 2, Number 4, April 10, 2026
ISSN 3066-7623 (online) 3066-7607 (print)

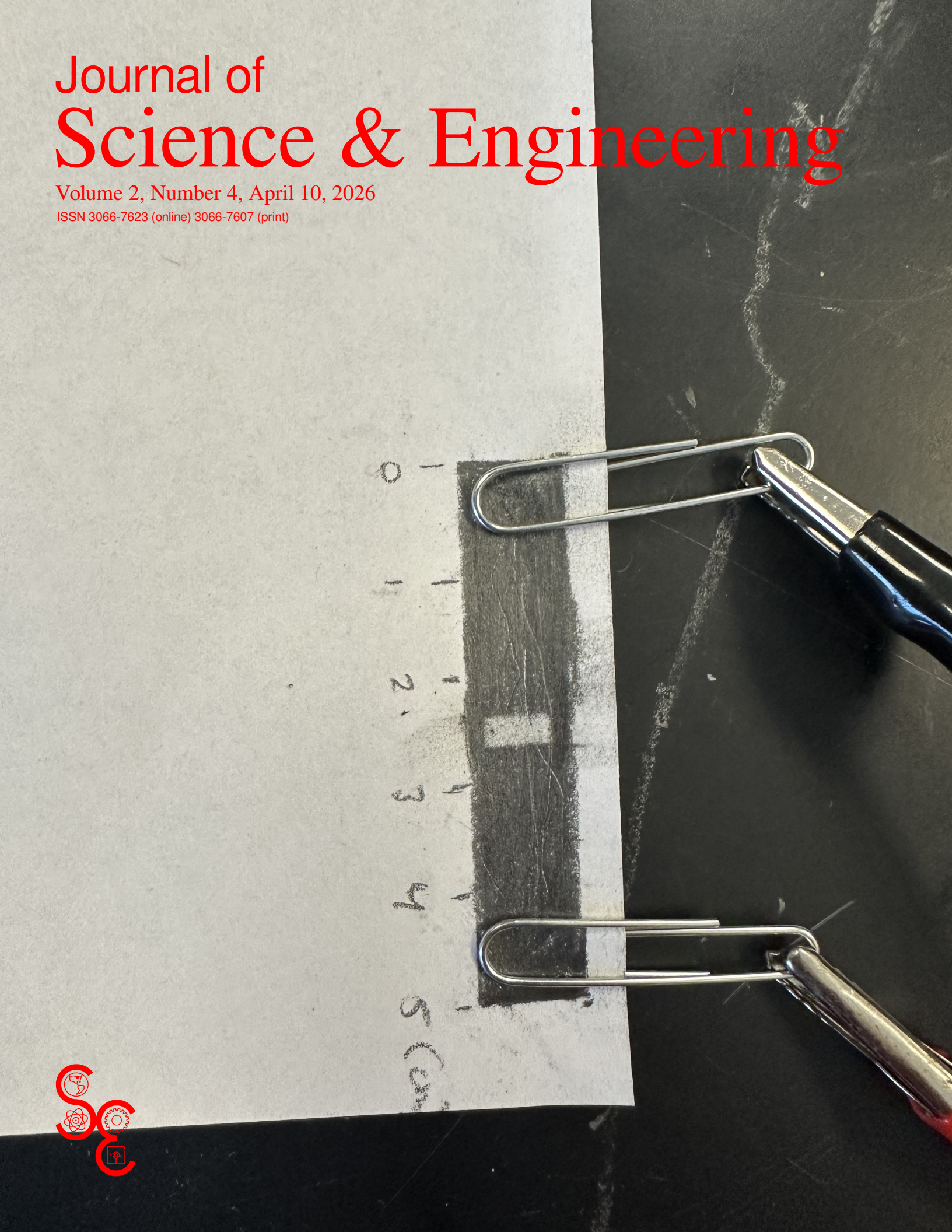

Journal of Science & Engineering (J S&E) publishes high quality, peer-reviewed, original research, short articles, articles, letters, and reports by promising students of science and engineering. J S&E is a publication of the Freehold Regional High School District Press. Our online ISSN is 3066-7623 and our print ISSN is 3066-7607. Metadata and digital object identifiers (DOI) for all fulltext articles are registered with Crossref. Our primary aim is to highlight science and engineering original research done by secondary students. An ancillary goal is to teach science/engineering communication, technical writing, and the peer review process to secondary students. J S&E is an open access journal.

Our editorial office is located at:

Journal of Science & Engineering
20 Church Lane Room G201
Englishtown, NJ 07726
United States

https://manalapan.frhsd.com/

https://sites.google.com/frhsd.com/seopenhouse/home

Journal of
Science & Engineering

Volume 2, Number 4, April 10, 2026

From the cover: Electrical conductivity could potentially be used as a means to perform non-destructive testing (NDT) of conductive 3D printed parts such as those made from metal or from conductive filament. As 3D printing technology improves and such materials become more available, means of ensuring quality will be needed. Here we examine issues in using conductivity and voltage measurements to accomplish NDT, through laboratory measurements on physical models as well as through computational studies. *Cover image: Tushaar Akula, Miguel Arenas, Cole Canada, Daivik Jajoo, Anton Lavrenov, and Timur Neyir.*

The metal sits still,
yet electricity flows,
to find flaws we can't.

Rishith Chandra Kilaru

Modeling internal defects in conductive materials using electric potential measurements

Dia Avalur, Nitika Kishore, and Anika Tokala

***Abstract*—In this project, a numerical model was developed to study how electric potential behaves inside a conductive material and how internal defects can affect its electrical response. The material was represented as a two-dimensional grid, where each grid corresponds to an electric potential. Using basic principles of electrical conduction, the system was modeled under steady-state conditions and solved numerically using a finite-difference approach to Laplace's equation. Boundary conditions were applied by setting one side of the grid to a high potential while the other sides were grounded. After getting a steady-state solution, an internal defect was introduced by blocking a small region of the grid to simulate an insulating flaw. The resulting potential distributions were compared before and after the defect was added. The results showed that the presence of an internal defect caused noticeable changes in the potential pattern. These findings suggest that electrical measurements taken at the surface of a conductive object can give information about internal features, which supports the use of electrical methods or non-destructive testing.**

***Index Terms*—electric potential, Laplace's equation, finite-difference method, numerical modeling, non-destructive testing, equipotential lines, equipotentials, electric field visualizations, electric field mapping**

I. Introduction

ELECTRICAL conduction in a material is determined by the relationship between electric field, current flow, and electric potential, as described by Ohm's law [1]. Variations in electric potential create an electric field, and this drives current through a conductive medium [2]. Charge is conserved and does not accumulate within the material at steady state. This leads to an equation for the potential, known as Laplace's equation. To computationally study this behavior, the conductive region can be represented as a 2D grid with uniform spacing. Here, each grid point corresponds to the electric potential at that specific location. Boundary conditions are applied by fixing the potential on certain edges of the grid, such as holding one side at a high potential while keeping the other sides grounded [2]. Solving Laplace's equation on this grid would produce the steady state potential distribution and form the basis for analyzing how the internal features can change the system's electrical response.

Previous researchers examined conduction in a saline solution meant to simulate a low-cost electrophoresis system for biological studies [3]–[7]. These studies used measurements of voltage to map the equipotentials and electric fields within a test geometry, however, none considered the use of computational methods. Here, we consider the finite difference method, in which derivatives are approximated as differences between potential values at neighboring computational nodes, e.g.

$$\frac{dV}{dx} \approx \frac{V_{n+1} - V_n}{x_{n+1} - x_n}. \tag{1}$$

Application of this principle to 2D conduction equations is described below.

As 3D printers capable of metal and conductive materials become more available, low voltage DC electrical probing has potential advantages as a non-destructive testing (NDT) technique. Conventional techniques used in industry rely on x-rays from radioactive sources, pentrant dyes, or ultrasound equipment to accomplish NDT [8], [9], which may not be feasible for small-scale 3D printing setups. Methods based on conductivity have been applied to larger geophysical problems as well [10].

II. Methods and Materials

To model the electric potential inside the conductive region, Laplace's equation was solved using a finite-difference method on a two-dimensional grid [11]. The region was evenly divided into grid points, with each point representing the electric potential at that place. Boundary conditions were applied by fixing the potential along the edges of the grid, with one side held at a higher potential than the rest.

In a steady-state conductive material, no charge accumulates within the region because all charge is conserved [2], [12]–[14]. The continuity equation expresses this condition:

$$\vec{\nabla} \cdot \vec{J} = 0, \tag{2}$$

where $\vec{J}$ is the current density. Current density and electrical field are related through Ohm's law, expressed in differential form as [2]

$$\vec{J} = \sigma \vec{E}, \tag{3}$$

and the electric field is related to the electric potential by

$$\vec{E} = -\vec{\nabla}\phi. \tag{4}$$

These relationships combine, assuming the material has uniform conductivity, giving Laplace's equation [2]:

$$\vec{\nabla}^2 \phi = 0, \tag{5}$$

where the zero on the right hand side of (5) indicates the absence of internal sources. This equation controls the electric potential throughout the conductive region. In discretized form, (5) becomes [11]:

$$\frac{V_E - 2V_X + V_W + V_N - 2V_X + V_S}{h^2} = 0, \tag{6}$$

Author for correspondence: 426davalur@frhsd.com
Authors are with the Science & Engineering Magnet Program, Manalapan High School, 20 Church Lane, Englishtown, NJ 07726, USA

10.64804/9wkhqz81

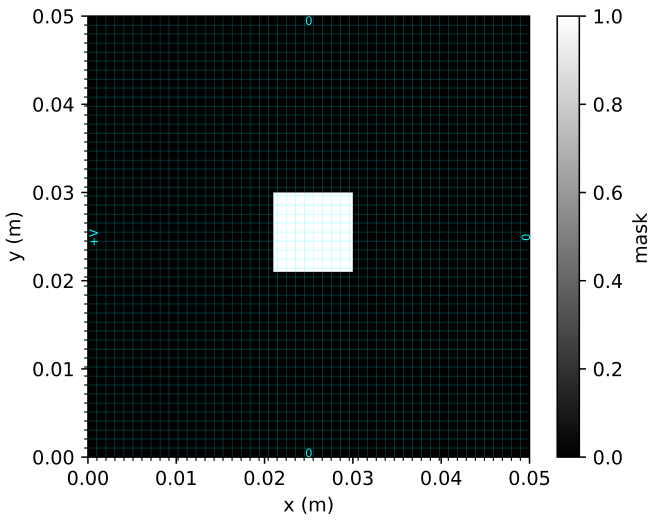

Fig. 1. Uniform regular square computational grid and pinned boundary conditions.

$$4V_X = V_E + V_W + V_N + V_S, \tag{7}$$

where a given node point V_X is adjacent to neighbors north, south, east, and west on a regular grid of uniform spacing h. We iteratively calculated V by setting each interior point equal to the average of its four surrounding points. The process was repeated for 5000 iterations. As a convergence check during development, the mesh size was decreased and iterations increased tenfold with no change to results.

III. Computational Model

The conductive material was represented using a two-dimensional grid. The grid consisted of a 50×50 array, with the left boundary held at a high potential and the other boundaries grounded. Each point on the grid corresponds to the electric potential at that location, and the grid as a whole acts as a simplified model of the material. This allows the electric behavior of the system to be studied numerically instead of analytically.

Boundary conditions were applied by fixing the potential values along the edges of the grid. One side of the grid was set to a high potential to represent an applied voltage, while the remaining sides were set to ground. These fixed boundaries remained constant throughout the course of the simulation, while the interior grid points were free to update.

The potential values at the interior points were iteratively updated based on their surrounding neighbors until the grid itself reached a steady state. This steady-state solution represents how the electric potential would distribute itself throughout the material under the applied boundary conditions. By modifying the grid, such as introducing an internal blocked region to represent a defect, changes in the overall electrical response of the system can be observed. The computational grid and boundary conditions used in this model are shown in Fig. 1.

IV. Procedures

First, the basic physical principles controlling electrical conduction were identified. Ohm's law was used to relate current flow to the electric field, and the electric field was related to electric potential. Since charge does not accumulate in a steady-state system, these relationships combine and produce Laplace's equation, which describes how electric potential behaves inside a uniform conductive material.

To model this behavior computationally, the conductive material was represented using a Python program as a two-dimensional square grid. The grid was implemented as a 50×50 `numpy` array [15], where each element corresponds to the electric potential at a specific location in the material. Pinned boundary conditions were applied by directly assigning fixed potential values to the grid edges. One side of the grid was set to a high potential in order to represent an applied voltage, while the other sides were set to zero to represent ground. These boundary values were held constant throughout the simulation.

The interior points of the grid were solved using an iterative finite-difference method. In the beginning, the potential at every interior point was updated to equal the average of its four closest neighboring points. This update was performed using nested loops in the code, while skipping the boundary points so their values stayed fixed. The update process was repeated for several thousand iterations until the potential value changes became negligible, which indicated that a steady-state solution was reached.

Once the baseline solution was obtained, an internal defect was introduced into the model. This defect was represented by choosing a small square portion near the center of the grid and stopping those points from being updated during the iteration process. In the code, this was handled using a conditional statement that excluded the defect section from the averaging step. This region behaved as an insulating flaw within the material. The technique used here created a pinned boundary condition at the flaw with the nodes fixed at their initial values. Strictly speaking, this is not a no-flow boundary as might be expected for a nonconductive void; however, due to the location of the flaw at the centerline it behaves approximately the same way.

Lastly, the simulation results were visualized using `matplotlib` [16]. Heatmaps were generated to show the steady-state potential distribution for both the intact material and the material containing the defect. A difference plot was also created by subtracting the baseline potential grid from the defect grid. This showed how the defect changed the overall potential distribution.

Data and code are available at https://github.com/devangel77b/426davalur-lab10.

V. Results

After running the simulation, the electric potential across the grid settled into a smooth pattern from the high-voltage side toward the sides that are grounded. This is what we expect from a solution to Laplace's equation with pinned boundary conditions, and it showed that the numerical method was

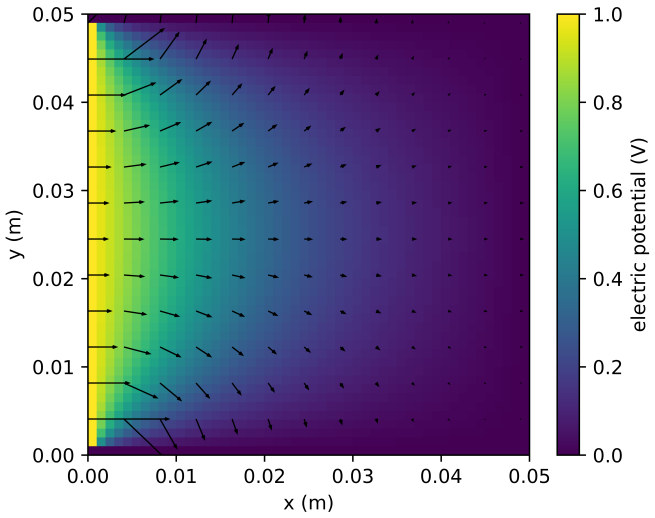

Fig. 2. Steady-state potential distribution (no defect) and electric field vectors.

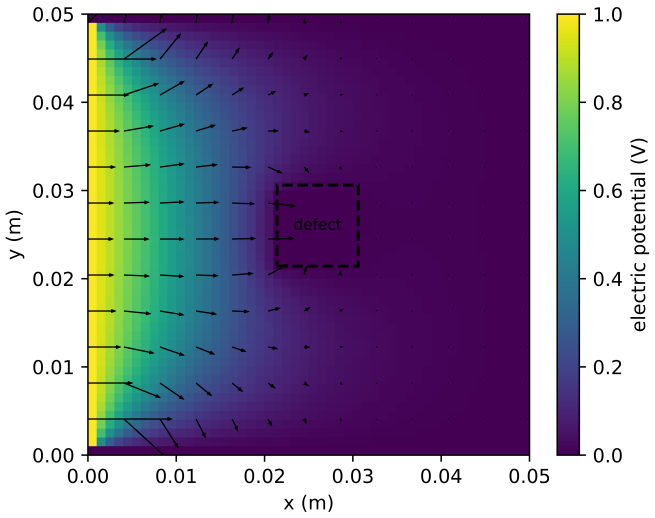

Fig. 3. Steady-state potential distribution and electric field vectors with internal defect.

working correctly. The potential values stopped changing after multiple iterations, indicating that the system had reached a steady state. This electrical potential distribution obtained from the simulation is shown in Fig. 2.

When a defect was added by blocking a small portion of the grid, the potential pattern changed. The values around the defect were distorted, and this disturbance spread outward toward the grid edges. The resulting electric potential distribution with the defect present is shown in Fig. 3.

Comparing the boundary values before and after adding the defect showed noticeable differences in a region of about two- to three times the length of the flaw. This suggests that changes in the material can be detected by only looking at measurements taken along the surface.

VI. Discussion

The results of this simulation show that internal changes within a conductive material can influence the electrical behavior observed at its surface. Even though the defect was located in the grid, its presence still altered the potential near the boundaries. This is important because it means that information about the interior of a material can be inferred without directly accessing it, which is the main idea behind non-destructive testing [10], [17].

The distortion caused by the defect was not limited to the immediate area around it. Instead, the effect spread outward and affected the overall potential pattern to a distance of 2 to 3 times the length of the flaw. This suggests that electrical measurements taken at the surface are sensitive to internal features. Even when those features are not visible or are relatively small.

Even though this model is simplified, it captures the behavior of steady-state electrical conduction. The fact that a basic grid-based simulation is able to show these effects support the idea that electrical probing can be a useful tool for detecting internal mistakes. More detailed models could likely improve accuracy, but the trends observed are consistent with the expected physical behavior.

A. Limitations

This model uses many simplifying assumptions that limit how closely it represents a real physical system. The simulation is two-dimensional, while real conductive objects are three-dimensional, which means that some effects present in real materials are not captured here. The conductivity of the material is also assumed to be uniform, even though real materials can have variations that affect current flow. Also, the defect is represented as a completely blocked region, which is a simplified way of modeling an internal flaw. Lastly, the grid resolution is limited, so very detailed or small figures may not be accurately represented. These limitations are illustrated in Fig. 4, which shows that the effect of the defect appears as a broad change in the potential rather than a defined feature.

B. Detectability limits of internal defects

An important question is how defect size and material properties affect whether a flaw can be detected from surface measurements. In this model, the defect was big enough to clearly distort the potential, but smaller defects would produce weaker, more localized changes that may not be visible at the boundaries.

Material conductivity also plays a role. In highly conductive materials, current can redistribute more easily around a defect, reducing its effect on the surface potential. Also, this model does not include noise or measurement limitations, so it likely overestimates how detectable a defect would be in practice.

Overall, while defects do influence surface measurements, their detectability depends on both their size and the material properties, and smaller defects may not always be observable.

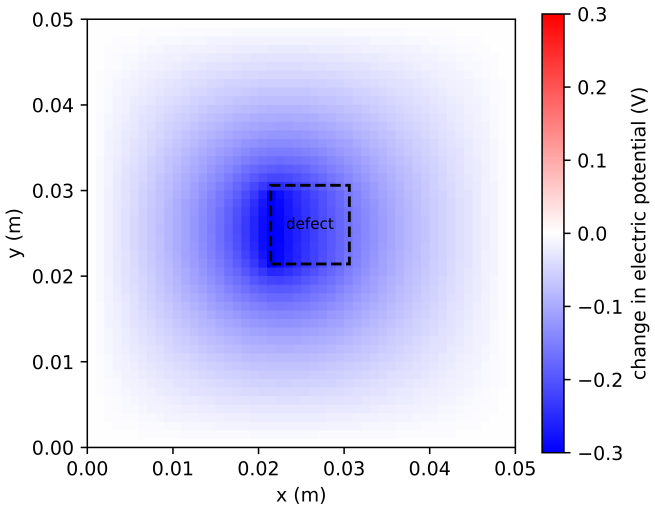

Fig. 4. Difference in electric potential due to an internal defect.

C. Conclusion

This project showed that a simple numerical model can still reveal meaningful information about how electricity behaves in a conductive material. By modeling the material as a grid and solving for the steady-state potential, it became clear that internal changes, like an insulating defect, can affect the electrical behavior seen at the surface. Even with a basic setup, the defect caused noticeable distortions in the potential pattern, especially near the boundaries. This supports the idea that electrical measurements taken at the surface can be used to learn about what is happening inside a material. Overall, this model provides a clear example of how numerical methods can be used to explore non- destructive testing concepts in a straightforward and effective way.

APPENDIX

This code is available at https://github.com/devangel77b/426davalur-lab10. Relaxation is implemented at approximately line 60. Line 58 implements pinned nodes for a centerline defect.

```python
import numpy as np
import matplotlib.pyplot as plt
from matplotlib.patches import Rectangle



# ----------------------------
# Settings
# ----------------------------
N = 50 # grid dimensions N x N
ITERATIONS = 5000 # number of relaxation iterations
V_HIGH = 1.0 # high potential boundary value
V_GROUND = 0.0 # grounded boundary value
# Defect settings (squre block in the center)
DEFECT_HALF_WIDTH = 4 # defect will be (2*half_width+1) by (2*half_width+1)
# Physical size of square domain (meters)
Lx = 0.05
Ly = 0.05



# ----------------------------
# Helper: apply boundary conditions
# ----------------------------
def apply_boundary_conditions(V: np.ndarray) -> None:
    """
    Left boundary = high potential
    All other boundaries = grounded
    """
    V[:, 0] = V_HIGH # left = high
    V[:, -1] = V_GROUND # right = ground
    V[0, :] = V_GROUND # top = ground
    V[-1, :] = V_GROUND # bottom = ground









# ----------------------------
# Solver: finite difference relaxation
# ----------------------------
def solve_laplace(N: int, iterations: int, defect_mask: np.ndarray | None = None) -> np.ndarray:
    """
    Solves Laplace's equation on an N x N grid using iterative relaxation.
    If defect_mask is provided, True cells are treated as blocked and not updated.
    """
    V = np.zeros((N, N), dtype=float)
    apply_boundary_conditions(V)
    for _ in range(iterations):
        # update interior points
        for i in range(1, N - 1):
            for j in range(1, N - 1):
                if defect_mask is not None and defect_mask[i, j]:
                    continue
                V[i, j] = 0.25 * (
                    V[i + 1, j] +
                    V[i - 1, j] +
                    V[i, j + 1] +
                    V[i, j - 1]
                )
        # reapply boundary conditions each iteration just to be safe
        apply_boundary_conditions(V)
    return V









# ----------------------------
# Make defect mask
# ----------------------------
def make_center_defect_mask(N: int, half_width: int) -> np.ndarray:
    """
    Creates a square defect mask in the center.
    True = defect region
    """
    mask = np.zeros((N, N), dtype=bool)
    c = N // 2
    mask[
        c - half_width:c + half_width + 1,
        c - half_width:c + half_width + 1
    ] = True
    return mask









# ----------------------------
# Compute electric field
# ----------------------------
def compute_electric_field(V: np.ndarray, Lx: float, Ly: float):
    """
    Computes E = -grad(V)
    """
    dx = Lx / (V.shape[1] - 1)
    dy = Ly / (V.shape[0] - 1)
    dVdy, dVdx = np.gradient(V, dy, dx)
```

```
    Ex = -dVdx
    Ey = -dVdy
    return Ex, Ey




# ----------------------------
# Figure 1: discretized grid, boundary conditions, and mask
# ----------------------------
# mask
def save_mask(
        mask: np.ndarray,
        filename : str,
        cmap: str = "gray") -> None:
    x = np.linspace(0, Lx, mask.shape[1])
    y = np.linspace(0, Ly, mask.shape[0])
    X, Y = np.meshgrid(x,y)
    plt.figure(figsize=(5,4))
    ax = plt.gca()
    im = ax.imshow(
        mask,
        cmap=cmap,
        origin="lower",
        extent=[0, Lx, 0, Ly],
        aspect="equal",
        vmin=0,
        vmax=1
    )
    plt.text(0.025, 0.049, "0",
    ↪  ha="center",color=(0,1,1),fontsize=6)
    plt.text(0.025, 0, "0",
    ↪  ha="center",color=(0,1,1),fontsize=6)
    plt.text(0.049, 0.025, "0", rotation=90,
    ↪  va="center",color=(0,1,1),fontsize=6)
    plt.text(0, 0.025, "+V", rotation=90,
    ↪  va="center",color=(0,1,1),fontsize=6)
    ax.set_xticks(x,minor=True)
    ax.set_yticks(y,minor=True)

    ↪  ax.grid(which='minor',color=(0,1,1),linestyle='-',linewidth=0.1)
    cbar = plt.colorbar(im, ax=ax)
    cbar.set_label("mask")
    ax.set_xlabel("x (m)")
    ax.set_ylabel("y (m)")
    plt.tight_layout()
    plt.savefig(filename, dpi=1200, bbox_inches="tight")
    plt.close()




# ----------------------------
# Heatmap + vector field
# ----------------------------
def save_heatmap_with_field(
        V: np.ndarray,
        filename: str,
        cmap: str = "viridis",
        defect_mask: np.ndarray | None = None,
        annotate_defect: bool = False
) -> None:
    Ex, Ey = compute_electric_field(V, Lx, Ly)
    # coordinate grid in meters
    x = np.linspace(0, Lx, V.shape[1])
    y = np.linspace(0, Ly, V.shape[0])
    X, Y = np.meshgrid(x, y)
    plt.figure(figsize=(5, 4))
    ax = plt.gca()
    im = ax.imshow(
        V,
        cmap=cmap,
        origin="lower",
        extent=[0, Lx, 0, Ly],
        aspect="equal",
        vmin=0,
        vmax=1
    )
    cbar = plt.colorbar(im, ax=ax)
    cbar.set_label("electric potential (V)")

    # Subsample arrows so plot isn't overcrowded
    step = 4
    Xq = X[::step, ::step]
    Yq = Y[::step, ::step]
    Exq = Ex[::step, ::step]
    Eyq = Ey[::step, ::step]

    # If defect exists, do not draw arrows inside it
    if defect_mask is not None:
        maskq = defect_mask[::step, ::step]
        Exq = np.where(maskq, np.nan, Exq)
        Eyq = np.where(maskq, np.nan, Eyq)
    ax.quiver(
        Xq, Yq, Exq, Eyq,
        color="black",
        #scale=10,
        width=0.003,
        headwidth=3,
        headlength=4
    )

    # Draw defect box if present
    if defect_mask is not None:
        rows, cols = np.where(defect_mask)
        i_min, i_max = rows.min(), rows.max()
        j_min, j_max = cols.min(), cols.max()

        dx = Lx / (V.shape[1] - 1)
        dy = Ly / (V.shape[0] - 1)
        x0 = j_min * dx
        y0 = i_min * dy
        width = (j_max - j_min + 1) * dx
        height = (i_max - i_min + 1) * dy
        rect = Rectangle(
            (x0, y0), width, height,
            linewidth=1.5,
            edgecolor="black",
            facecolor="none",
            linestyle="--"
        )
        ax.add_patch(rect)

        if annotate_defect:
            ax.text(
                x0 + width / 2,
                y0 + height / 2,
                "defect",
                color="black",
                fontsize=8,
                ha="center",
                va="center"
            )

    ax.set_xlabel("x (m)")
    ax.set_ylabel("y (m)")
    plt.tight_layout()
    plt.savefig(filename, dpi=1200, bbox_inches="tight")
    plt.close()




# ----------------------------
# Difference map
# ----------------------------
def save_difference_map(
        deltaV: np.ndarray,
        filename: str,
        defect_mask: np.ndarray | None = None,
        annotate_defect: bool = False) -> None:
    plt.figure(figsize=(5, 4))
    ax = plt.gca()
    im = ax.imshow(
        deltaV,
        cmap="bwr",
        origin="lower",
        extent=[0, Lx, 0, Ly],
        aspect="equal"
    )

        # Draw defect box if present
    if defect_mask is not None:
        rows, cols = np.where(defect_mask)
        i_min, i_max = rows.min(), rows.max()
        j_min, j_max = cols.min(), cols.max()

        dx = Lx / (deltaV.shape[1] - 1)
        dy = Ly / (deltaV.shape[0] - 1)
        x0 = j_min * dx
        y0 = i_min * dy
```

```
        width = (j_max - j_min + 1) * dx
        height = (i_max - i_min + 1) * dy
        rect = Rectangle(
            (x0, y0), width, height,
            linewidth=1.5,
            edgecolor="black",
            facecolor="none",
            linestyle="--"
        )
        ax.add_patch(rect)

        if annotate_defect:
            ax.text(
                x0 + width / 2,
                y0 + height / 2,
                "defect",
                color="black",
                fontsize=8,
                ha="center",
                va="center"
            )

    im.set_clim(-0.3,0.3)
    cbar = plt.colorbar(im, ax=ax)
    cbar.set_label("change in electric potential (V)")
    ax.set_xlabel("x (m)")
    ax.set_ylabel("y (m)")
    plt.tight_layout()
    plt.savefig(filename, dpi=1200, bbox_inches="tight")
    plt.close()




# ----------------------------
# Main
# ----------------------------
def main():
    # Figure 1
    #save_figure1_grid_setup("Figure1_GridSetup.png", N)

    # No defect
    V_base = solve_laplace(N, ITERATIONS)
    save_heatmap_with_field(
        V_base,
        "Figure2_BaselinePotential.png",
        cmap="viridis"
    )

    # With defect
    defect_mask = make_center_defect_mask(N,
    ↪  DEFECT_HALF_WIDTH)
    V_defect = solve_laplace(N, ITERATIONS,
    ↪  defect_mask=defect_mask)
    save_heatmap_with_field(
        V_defect,
        "Figure3_DefectPotential.png",
        cmap="viridis",
        defect_mask=defect_mask,
        annotate_defect=True
    )

    # Difference map
    deltaV = V_defect - V_base
    save_difference_map(
        deltaV,
        "Figure4_PotentialDifference.png",
        defect_mask=defect_mask,
        annotate_defect=True
    )

    # defect mask
    save_mask(defect_mask,"Figure1_mask.png")

    print("Done. Generated Figure1{Figure4 PNG files.")




if __name__ == "__main__":
    main()
```

ACKNOWLEDGMENT

We thank the Manalapan High School Science & Engineering program for their support. We thank several anonymous reviewers for helpful feedback. DA developed the computational model, implemented the numerical simulation, and performed the analysis of the results. NK helped with developing the numerical approach, helped test and verify the simulation results, and contributed to editing and revising the written sections. AT supported the project by reviewing the model setup, helping with interpretation of the results, and providing feedback during the writing process.

REFERENCES

[1] R. D. Knight, *Physics for Scientists and Engineers: a strategic approach*, 4th ed. Pearson, 2017.
[2] J. D. Jackson, *Classical Electrodynamics*, 3rd ed. John Wiley & Sons, 1999.
[3] S. Ayyagari, V. Collemi, K. Shah, and K. Tomazic, "Computational mapping analysis of equipotential and electric field lines in gel electrophoresis rig," *Journal of Science & Engineering*, vol. 1, pp. 37–40, 2024.
[4] S. Baru, V. Choudhary, P. Thaker, N. Martin, and D. Ahmad, "Demonstrating a method to create a low-cost electrophoresis rig solution," *Journal of Science & Engineering*, vol. 1, pp. 42–44, 2024.
[5] R. Cohen, S. Musuku, J. Hammer, E. Handique, N. Patel, D. Gandhi, and N. Gershteyn, "Visualizing electric potential: mapping equipotential lines in a conductive water tray," *Journal of Science & Engineering*, vol. 1, pp. 45–47, 2024.
[6] R. Edwards, C. Karabin, C. Li, K. Patel, and J. Schatz, "Electric field mapping for cost-effective gel electrophoresis applications," *Journal of Science & Engineering*, vol. 1, pp. 49–52, 2024.
[7] A. Kumar, S. Perkins, N. Muthukumar, H. Villaseñor, and A. Khanna, "Mapping electric potential and electric field distribution in saltwater and investigating the effect of distance from source," *Journal of Science & Engineering*, vol. 1, pp. 53–55, 2024.
[8] J. R. Davis, *Non-Destructive Evaluation of Materials*. Materials Park, OH: ASM International, 2004.
[9] P. Cawley, "Non-destructive testing—current capabilities and future directions," *Proceedings of the Institution of Mechanical Engineers, Part L: Journal of Materials: Design and Applications*, vol. 215, pp. 213–223, 2001.
[10] M. H. Loke, J. E. Chambers, D. F. Rucker, O. Kuras, and P. B. Wilkinson, "Recent developments in the direct-current geoelectrical imaging method," *Journal of Applied Geophysics*, vol. 95, pp. 135–156, 2013.
[11] W. H. Press, S. A. Teukolsky, W. T. Vetterling, and B. P. Flannery, *Numerical Recipes in C: the art of scientific computing*, 2nd ed. Cambridge University Press, 1992.
[12] R. A. Pelcovits and J. Farkas, *Barron's AP Physics C Premium*. Fort Lauderdale, FL: Kaplan North America, 2024.
[13] P. A. Tipler and G. Mosca, *Physics for Scientists and Engineers*, 5th ed. New York: W H Freeman and Company, 2004.
[14] W. Moebs, S. J. Ling, and J. Sanny, *University Physics*. Houston, TX: OpenStax, 2016, vol. 1.
[15] C. R. Harris, K. J. Millman, S. J. van der Walt, R. Gommers, P. Virtanen, D. Cournapeau, E. Wieser, J. Taylor, S. Berg, N. J. Smith, R. Kern, M. Picus, S. Hoyer, M. H. van Kerkwijk, M. Brett, A. Haldane, J. F. del Río, M. Wiebe, P. Peterson, P. Gérard-Marchant, K. Sheppard, T. Reddy, W. Weckesser, H. Abbasi, C. Gohlke, and T. E. Oliphant, "Array programming with NumPy," *Nature*, vol. 585, pp. 357–362, 2020.
[16] J. D. Hunter, "Matplotlib: A 2d graphics environment," *Computing in Science & Engineering*, vol. 9, pp. 90–95, 2007.
[17] A. Hauptmann, M. Ikehata, H. Itou, and S. Siltanen, "Revealing cracks inside conductive bodies by electric surface measurements," *Inverse Problems*, vol. 35, p. 025004, 2018.

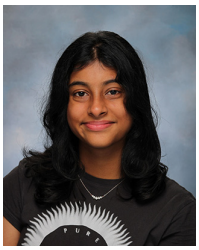

Dia Avalur is a senior in the Science and Engineering Magnet Program at Manalapan High School. Her main area of research is the intersection between engineering and medicine, including the development of alginate patches for drug delivery, early detection of neurological conditions from machine learning, and studies of segmentation in medical imaging.

Nitika Kishore is a senior in the Science and Engineering Magnet Program at Manalapan High School. Her main area of research is the wonderful world of lasers. When she is not studying AP Physics C E&M she enjoys developing low-cost intravenous monitoring devices and breathtaking laser light shows that turn it up to 11.

Anika Tokala is a senior in the Science and Engineering Magnet Program at Manalapan High School. Her main area of research is accessibility technology. When she is not studying AP Physics C E&M she enjoys literature and developing screen readers to assist blind and visually impaired students with math.

Detecting flaws in metal by mapping equipotentials on a two-dimensional graphite model

Callie Butash, Emily Chen, Jake Chin, Jason Donovan Katz, Grace Nealon, and Petra Rofman

***Abstract*—With the popularization of 3-D (three-dimensional) printed metals, the necessity for a method to detect internal flaws is increasing. We experimented with a 2-D (two-dimensional) graphite model of 3-D printed metal and measured the potential at various points throughout the model in a grid-like fashion. To simulate imperceptible flaws, we erased internal portions of the graphite and re-measured the potentials at the same points. Graphing our measurements, we created representations of nonlinear potential differences, allowing us to conclude that calculating potential in intervals over a conducting surface is a valid method to detect imperfections hidden within 3-D printed conducting surfaces under certain conditions.**

***Index Terms*—equipotentials, two-dimensional, voltage, electric potential, electric field, graphite, three-dimensional (3-D), two-dimensional (2-D), non-destructive testing**

I. Introduction

THE ELECTRIC POTENTIAL of a particle can be described as the amount of electric potential energy per unit column of charge [1]–[3]. This can be represented by the following equation:

$$\Delta V = -\int \vec{E} \cdot d\vec{r}, \tag{1}$$

where V is the potential difference that is represented by the integral of the electric field along a path, with the negative sign showing that electric potential will decrease in the direction of the field. Equipotential lines represent locations in an electric field where the potential is constant [4], [5]. We want to decipher how an electric field will differ when given a vertical or a horizontal gap utilizing measured potential and (1). Previous research in this area has examined mapping equipotentials and electric fields for low-cost electrophoresis cells [6]–[10], thus the technique has potential for our current application.

As more capable additive manufacturing (i.e. 3D printing) technologies become more widely available, including in conductive materials such as metal, means of testing the integrity of parts nondestructively (non-destructive testing or NDT) are needed. Traditional industrial methods for NDT require specialized equipment (ultrasonic testing), radioactive sources (radiographic testing), or chemical dyes (penetrant testing), all of which would be unwieldy for small scale 3D printing processes [11], [12]. Researchers have been finding defects in 3-D printed metal using x-ray imaging, heat cameras, and AI machine learning [13]–[15]. While their advanced technologies offer high-quality options to detect these flaws, our 2-D model is a more cost-effective and accessible option. Our solution utilizes potentials and the electric field and offers a quick quality check of the metals rather than an in-depth location search.

We hypothesize that blemishes in metal can be detected by observing a nonlinear voltage difference across a conducting surface. Since electric fields run perpendicular to equipotentials we expect that in the solid graphite region, the equipotentials will be linear, and perpendicular to the electric field. We also expect that at all grid points in the region with a vertical flaw will have nonlinear equipotential lines that run horizontally and curve around the discontinuity. Finally, we expect that the region with a horizontal flaw will have relatively linear equipotential lines. As the grid points get closer to where the flaw is located, the equipotential lines for this region may begin to curve around the discontinuity.

To test these hypotheses, we set up an experiment to replicate, in two dimensions, the voltage across a conductive material: graphite. Our experiment models a block of metal as a graphite square on paper and flaws as erased portions. We conducted three trials: unflawed metal, metal with a vertical flaw, and metal with a horizontal flaw.

II. Methods and Materials

A. Setup

To test our hypotheses, we used a ruler to measure a box with dimensions $50\,\mathrm{mm} \times 50\,\mathrm{mm}$ on the corner of $8.5\,\mathrm{inch} \times 11\,\mathrm{inch}$ printer paper and marked along the length and width of the box in increments of $10\,\mathrm{mm}$. We then shaded the box as darkly and uniformly as possible with the graphite from a standard #2 pencil (Dixon Ticonderoga; Appleton, WI).

Two paper clips were straightened, placed along opposite sides of the box, and attached to an adjustable power supply (WeFomey $3\,\mathrm{V}$ to $36\,\mathrm{V}$ $4\,\mathrm{A}$ $144\,\mathrm{W}$ Universal Power Supply; Amazon; Seattle, WA) operated at $5\,\mathrm{V}$. The paperclips ensured good electrical contact. The negative lead from the battery pack was wrapped around the paperclip at the top of the square, and the positive lead was wrapped around the paperclip at the bottom. We used masking tape to secure the wires and paper clips to the paper surface.

B. Data collection

Using a digital multimeter (Fluke 106; Everett, WA), we measured the voltages with the negative probe on the negatively charged paper clip and the positive probe on the $10\,\mathrm{mm}$

Author for correspondence: 426cbutash@frhsd.com
Authors are with the Science & Engineering Magnet Program, Manalapan High School, 20 Church Lane, Englishtown, NJ 07726, USA

10.64804/9hz16085

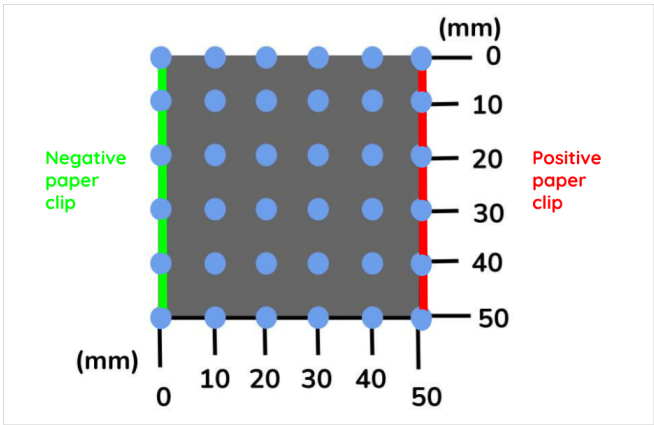

Fig. 1. Graphite square for control trial with grid.

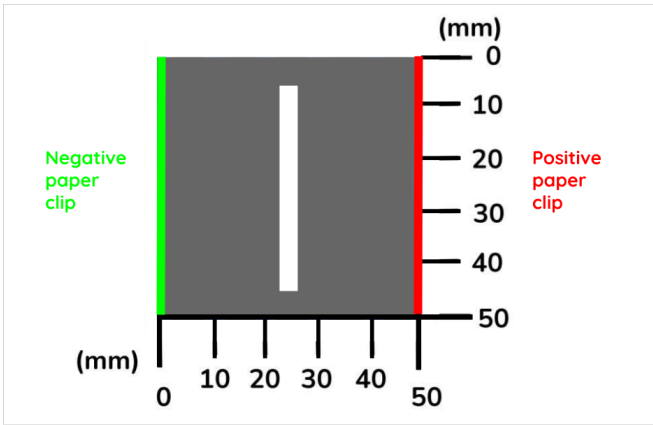

Fig. 2. Graphite square for trial with horizontal flaw.

mark at the leftmost edge of the graphite square. Keeping the negative probe in place, we moved the positive probe to the right along the graphite in increments of $10\,\mathrm{mm}$ until we reached the rightmost edge at $50\,\mathrm{mm}$ and recorded the resulting voltage. We repeated this across each row of $10\,\mathrm{mm}$ increments until we had voltage values for all intersections of $10\,\mathrm{mm}$ grid lines, depicted as light blue dots in Fig. 1.

C. Horizontal and vertical flaws

To mimic flaws in the metal, we erased a vertical line halfway through the box, spanning a length of $45\,\mathrm{mm}$ and a width of approximately $5\,\mathrm{mm}$, as shown in Fig. 2, to create a horizontal flaw. We repeated the aforementioned experimental process to record the voltage throughout the box in the same grid-like fashion. Then, we moved the paperclips to the two other sides of the box, causing the same erased "flaw" to be vertical, as shown in Fig. 3, and repeated the process of measuring the voltage throughout the box in the same grid-like fashion.

The flaw orientation is potentially important for NDT applications as different techniques are sensitive to flaws in particular orientations. For example, in traditional NDT, radiographic testing is most sensitive to flaws along the path of the x-rays; while ultrasonic testing is most sensitive to flaws the present a discontinuous interface normal to the beams [11], [12].

III. Results

A. Control

In our first experiment with a solid region (setup from Fig. 1), we had a fairly linear voltage difference across the graphite square. This is to be expected as the region is continuous, allowing the electric field to remain constant and the equipotential lines to be evenly spaced, as shown in Figs. 4 and 5.

The control trial demonstrates the relatively consistent potential measurements across each axis of the grid, providing a baseline measurement. If we didn't know if the grid had flaws or not, this is what would be expected for a solid square. The equipotentials and field lines are all perpendicular to each other, with the constant spacing demonstrating a consistent electric field.

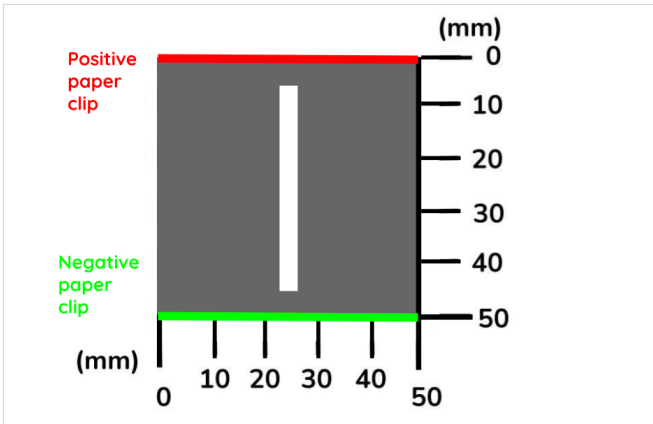

Fig. 3. Graphite square for trial with vertical flaw.

B. Horizontal flaw

In the region with a horizontal flaw (Fig. 2), we had a horizontal, linear voltage difference along the sides of the square with a center voltage of zero. This measurement lines up with the absence of graphite in that region. The graph of the potential difference (Fig. 6) highlights the interruption of measured voltage in the region where the flaw is located. The diagram of equipotential and electric field lines (Fig. 7) visualizes the effects of the gap on the grid. The distorted lines still fall perpendicular to each other, but in order to do so they bend around the void.

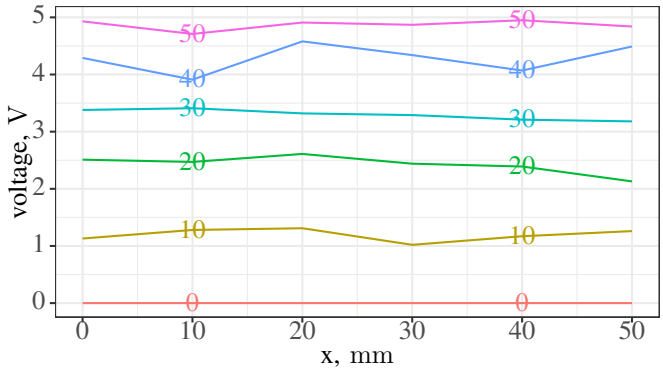

Fig. 4. Potential difference across the uniform graphite grid. Colors indicate y-transects spaced at 10 mm.

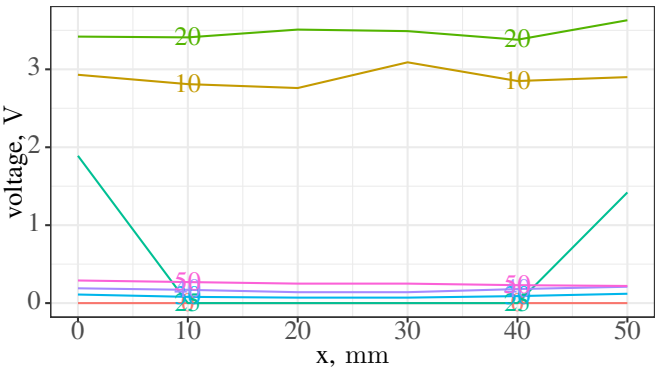

Fig. 6. Potential difference across the horizontally flawed grid. Colors indicate y-transects spaced at 10 mm.

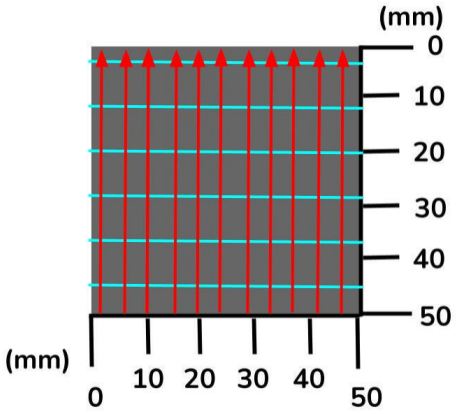

Fig. 5. Electric field (red) and equipotential lines (blue) across the uniform graphite grid.

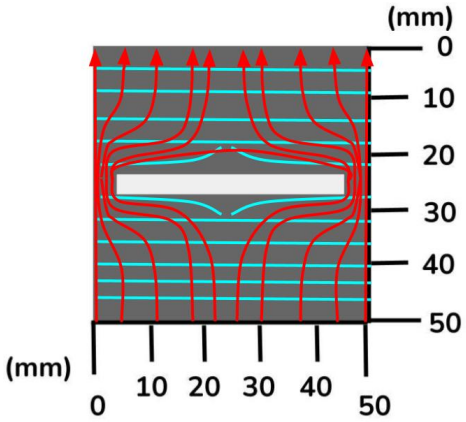

Fig. 7. Electric field (red) and equipotential lines (blue) across the horizontally flawed grid.

C. Vertical flaw

In the region with a vertical flaw (Fig. 3), we had a vertical, linear voltage difference along the sides of the square with a center voltage of zero, again in the location where graphite was erased. The graph of the potential difference (Fig. 8), however, fails to highlight the interruption in voltage in the region where the flaw is located. The visualization of the voltage and electric field (Fig. 9) demonstrates the distortion, which is noticeably less than in the horizontal flaw (Fig. 7).

IV. Discussion

A. Did the flaw cause a predictable effect on the measured potential values?

In this experiment, we successfully measured and mapped potential values across flawed and unflawed graphite squares to mimic flawed and unflawed 3-D printed metals. The voltage measurements change smoothly throughout the graphite squares, except when the measurements near the gaps.

Comparing the graphs of the potential difference, however, shows that only the horizontally flawed trial produced a graph visibly different from the control trial. Figs. 7 and 9 show how the orientation of the flaw affects the potential differences over the region. The potential with the horizontally flawed trial drops significantly after the flaw, as the imperfection in the surface increases resistance and, in turn, leads to a reduced voltage. Ultimately, when the flaw is parallel to the equipotentials, and perpendicular to the electric field, as in the horizontal setup of Fig. 9, current is much more disrupted, leading to more signal.

Our findings confirm that flaw orientation is important for NDT applications, similar to how traditional ultrasonic testing is most sensitive to flaws the present a discontinuous interface normal to the beams [11], [12].

B. Can we generalize our findings to find flaws in 3D printed metal?

Similarly to our 2-D model, defects in 3-D printed metal will cause varying paths in the electric field. Our findings lead us to believe that electrical testing can be generalized to identify if a 3-D printed conductor has flaws that are not visible on the surface. While the vertical flaw was more difficult

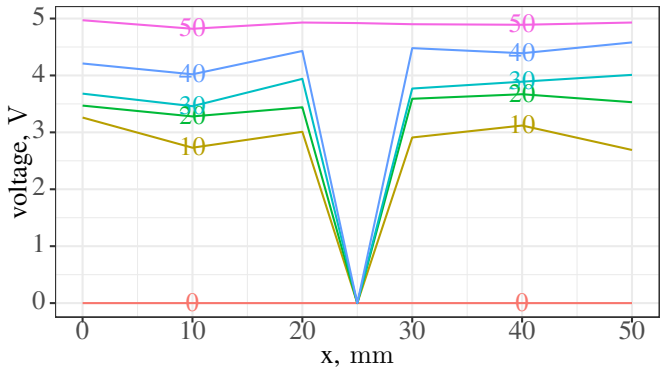

Fig. 8. Potential difference across the vertically flawed grid. Colors indicate y-transects spaced at 10 mm.

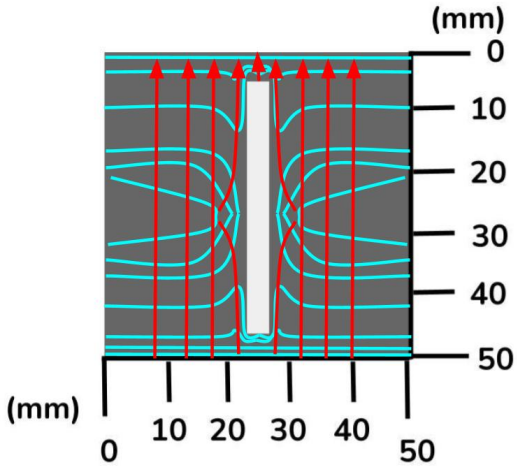

Fig. 9. Electric field (red) and equipotential lines (blue) across vertically flawed grid.

to detect than the horizontal one, there was still a gap in the potential measurements. In a similar manner to the 2-D experiment, a 3-D object can have a voltage source connected across it and have its voltage measured at varying points. Analysis of the voltage will find flaws located where there are abrupt changes. However, these items have an entirely new dimension introduced where the electric field lines can stray, meaning that it may be more difficult to identify these imperfections using potential than in 2-D due to the increased number of data points that would need to be collected to form an adequate grid. Furthermore, we believe that the difficulties we faced identifying flaws in different orientations in the 2-D model will be amplified.

C. Sources of experimental error

Inconsistent application of graphite to the box could change the resistance, where a thicker graphite patch would have a lower resistance and a thinner graphite patch would have a higher resistance, ultimately resulting in the voltage drop not being perfectly linear. Additionally, if the line wasn't perfectly erased, some current could still cross the remaining graphite, causing variations in the measured voltage. A last possible source of experimental error could be due to taking voltage measurements at inaccurate grid points; when eyeballing the grid points, the measurements may be slightly off their intended marks.

ACKNOWLEDGMENT

We thank the Science & Engineering program and several anonymous reviewers. CB created figures for lab setup and results, wrote the Discussion section and developed the Methods and Materials before the experiment. EC created the line charts for the results and wrote portions of the Introduction, Results, and Sources of Experimental Error sections. JC wrote portions of the Introduction, abstract, and Methods and Materials section. JK followed instructions by assisting and gathering measurements for the first trial, taking over for the other two, and making results diagrams. GN set up the experiment and took measurements for the first trials. She also crafted the Results section and worked on the Introduction. PR wrote the Methods and Materials section, as well as part of the abstract, Results, and Discussion sections.

REFERENCES

[1] P. A. Tipler and G. Mosca, *Physics for Scientists and Engineers*, 5th ed. New York: W H Freeman and Company, 2004.
[2] R. A. Pelcovits and J. Farkas, *Barron's AP Physics C Premium*. Fort Lauderdale, FL: Kaplan North America, 2024.
[3] W. Moebs, S. J. Ling, and J. Sanny, *University Physics*. Houston, TX: OpenStax, 2016, vol. 1.
[4] C. R. Nave, "Doing it by the numbers: Javascript calculations in web-based instructional material," in *AAPT Summer Meeting*, Guelph, Ontario, 2000, http://hyperphysics.phy-astr.gsu.edu/hbase/electric/equipot.html.
[5] R. D. Knight, *Physics for Scientists and Engineers: a strategic approach*, 4th ed. Pearson, 2017.
[6] S. Ayyagari, V. Collemi, K. Shah, and K. Tomazic, "Computational mapping analysis of equipotential and electric field lines in gel electrophoresis rig," *Journal of Science & Engineering*, vol. 1, pp. 37–40, 2024.
[7] S. Baru, V. Choudhary, P. Thaker, N. Martin, and D. Ahmad, "Demonstrating a method to create a low-cost electrophoresis rig solution," *Journal of Science & Engineering*, vol. 1, pp. 42–44, 2024.
[8] R. Cohen, S. Musuku, J. Hammer, E. Handique, N. Patel, D. Gandhi, and N. Gershteyn, "Visualizing electric potential: mapping equipotential lines in a conductive water tray," *Journal of Science & Engineering*, vol. 1, pp. 45–47, 2024.
[9] R. Edwards, C. Karabin, C. Li, K. Patel, and J. Schatz, "Electric field mapping for cost-effective gel electrophoresis applications," *Journal of Science & Engineering*, vol. 1, pp. 49–52, 2024.
[10] A. Kumar, S. Perkins, N. Muthukumar, H. Villaseñor, and A. Khanna, "Mapping electric potential and electric field distribution in saltwater and investigating the effect of distance from source," *Journal of Science & Engineering*, vol. 1, pp. 53–55, 2024.
[11] D. J. Griffiths, *Introduction to Electrodynamics*, 4th ed. Boston, MA: Pearson Education, 2013.
[12] C. Kittel, *Introduction to Solid State Physics*, 8th ed. Hoboken, NJ: Wiley, 2004.
[13] N. Forrester, "Researcher unveil new AI-driven method for improving additive manufacturing," https://www.anl.gov/article/researchers-unveil-new-aidriven-method-for-improving-additive-manufacturing, 2023.
[14] M. H. Loke, J. E. Chambers, D. F. Rucker, O. Kuras, and P. B. Wilkinson, "Recent developments in the direct-current geoelectrical imaging method," *Journal of Applied Geophysics*, vol. 95, pp. 135–156, 2013.
[15] A. Hauptmann, M. Ikehata, H. Itou, and S. Siltanen, "Revealing cracks inside conductive bodies by electric surface measurements," *Inverse Problems*, vol. 35, p. 025004, 2018.

Callie Butash is a senior in the Science and Engineering Magnet Program at Manalapan High School. She was an intern in Facilities Section of the Monmouth County Engineering Department. She is co-president of the Women in STEM Club. When she is not studying for AP Physics C E&M she enjoys soccer, track, and building a Spiderman-inspired grapple gun.

Emily Chen is a senior in the Science and Engineering Magnet Program at Manalapan High School. She is a member of the Drama Club. She is currently an intern at ACON Pharmaceuticals in Cranbury, NJ. When she is not studying for AP Physics C E&M she enjoys microspheres, musical theater, and working on her robotic fish.

Jake Chin is a senior in the Science and Engineering Magnet Program at Manalapan High School. He is a member of the Drama Club. He is currently an intern with Girl in Space Club and is developing web-based applications to teach students astrophysics and orbital mechanics of satellite swarms.

Jason Donovan Katz is a senior in the Science and Engineering Magnet Program at Manalapan High School. He is an avid tuba player and is president of the Beard Club. When he is not studying for AP Physics C E&M he enjoys aloha shirts and building robotic hands to play rock paper scissors. Upon graduation, he will begin studies at Mason Gross School of the Arts.

Grace Nealon is a senior in the Science and Engineering Magnet Program at Manalapan High School. She was an intern in the Traffic Section of the Monmouth County Engineering Department. She competes in track and lacrosse and is co-president of the Women in STEM Club. In her free time, she enjoys singing musical numbers at S&E Art and Science Night and building spy cars.

Petra Rofman is a senior in the Science and Engineering Magnet Program at Manalapan High School. She is a member of the Drama Club and the Rocketry Club. She is currently an intern at ACON Pharmaceuticals in Cranbury, NJ. When she is not studying for AP Physics C E&M she enjoys microspheres, origami, and working on her robotic fish.

Detecting defects in conductive graphite using voltage measurements

Tushaar Akula, Miguel Arenas, Cole Canada, Daivik Jajoo, Anton Lavrenov, and Timur Neyir

***Abstract*—Non-destructive testing (NDT) methods are critical for evaluating the reliability of mechanical components without damaging them. This is especially useful for applications like 3D printed metal and conductive parts, circuit testing, and detecting faults in electrical components. In this experiment, we use a uniform graphite surface from a No. 2 pencil to simulate a continuous 3D printed metal layer. A 9 V battery supplied an electric current through the graphite conductive medium and the voltage was measured at multiple points of the surface. A defect was mimicked on the graphite by erasing a rectangular portion of the graphite, and voltage was measured. For the uniform surface, voltage changed approximately linearly with distance, while the surface containing a defect showed a quick change in voltage at the gap. These results demonstrate that voltage measurements can be used to detect defects in conductive materials, supporting their application in non-destructive testing.**

***Index Terms*—electric potential, non-destructive testing, graphite conductor, voltage mapping, defect detection, conductive medium, electric field, resistance, discontinuity, circuit reliability**

I. Introduction

NON-DESTRUCTIVE testing (NDT) methods are critical for evaluating the reliability of mechanical components without damaging them, starting with the testing of the components' materials and metallic surfaces. As 3D printing technology advances and various methods become available to print in metal (e.g. powder bed fusion, direct energy deposition, and binder jetting with sintering), reliable, low-cost NDT methods for such parts will be needed. NDT techniques widely used in industry, such as penetrant testing, ultrasonic testing, and radiographic testing [1], [2], would be unwieldy for typical small-scale 3D printing workflows; thus we considered the use of electrical conductivity and voltage measurements [3], [4].

Previous researchers examined voltage measurements as a means to map equipotentials and electric fields inside an aqueous solution for application to a low-cost electrophoresis device [5]–[9]. The methods were low cost and could apply to a solid conductive medium like graphite [10].

In this experiment, an electric current flowed through a conductive medium, and electric potential was measured [11]–[17]. Defects were mimicked on the medium, and the electric potential was measured again and compared. This study demonstrates how electrical measurements can reveal flaws without damaging the material. The methods here could be performed on the sufrace of a 3D printed metal part, or within the body during the printing process as a quality assurance and process feedback step.

Author for correspondence: 226ccanada@frhsd.com
Authors are with the Science & Engineering Magnet Program, Manalapan High School, 20 Church Lane, Englishtown, NJ 07726, USA

10.64804/mzrrdy95

Background

A battery provides an electric potential difference, which establishes an electric field within a circuit. This electric field drives an electric current through a wire, whose resistance causes energy to be dissipated along the path. When an electric potential is applied to a continuous wire, the electric potential changes gradually along the length of the wire due to its resistance, as given by (1) and (2) [14]–[17]:

$$V = IR, \tag{1}$$

where V is voltage, I is current, and R is resistance, and

$$R = \frac{\rho l}{A}, \tag{2}$$

where ρ is the resistivity, l is the length and A is the cross-sectional area.

However, when the electric potential is interrupted by a discontinuity in the wire or any electrical component, charge can no longer move freely through that region [11], [12], [18]. This will create disruptions in a circuit, leading to unwanted failures. Instead, charge accumulates at the edges of the discontinuity, generating a strong electric field in the surrounding area. As a result, the current distribution near the discontinuity becomes uneven, with the current becoming more prominent near the edges. A significant localized voltage drop is also produced at this point due to the interruption in the wire. Therefore, by measuring the electric potential at different points along the wire, discontinuities can be identified by observing sudden and abnormal changes in electric potential. This is important to ensure that circuit components are not faulty, and circuits work as intended.

Even though these principles are often considered for metal wires, they could also be implemented for conductive surfaces like graphite [10] as well as for conductive polymers and for metals (powder or wire) depositing by 3D printing processes. In our experiment, graphite acts as our conductor. We seek to demonstrate that breaks, discontinuities, and defects in the surface can be detected by changes in voltage.

II. Methods and Materials

A. Graphite test surfaces

Test surfaces are shown in Fig. 1.

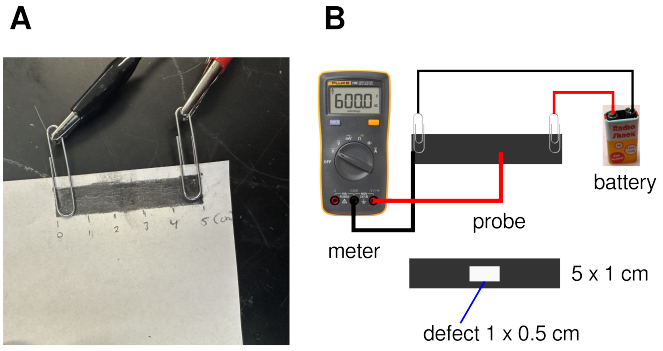

Fig. 1. Setup for measuring voltage across the graphite surfaces. (A) Uniform graphite surface 5 cm × 1 cm ready for testing. (B) Test connections to 9 V battery and meter.

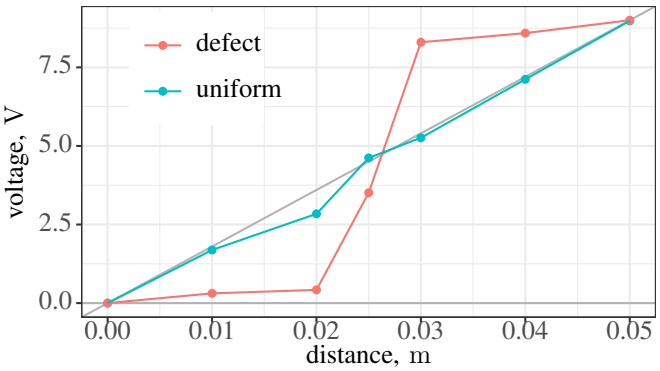

Fig. 2. Voltage vs. distance for the uniform (blue) and defect (pink) surface strips. A linearly increasing voltage, predicted for the uniform surface, is also shown in light gray. Surface geometry is as shown in Fig. 1; data from Tables I and II.

The conductive medium consisted of graphite deposited on paper using a No. 2HB pencil (S&E Teacher's Edition; Brooklyn, NY), forming a rectangular conductive region 0.05 m long and 0.01 m wide. A uniform graphite distribution was ensured by pressing down hard with the pencil so current could flow uniformly across the entire surface. Electrical contact was made at opposite ends of the graphite using paper clips connected to a 9 V battery. This supplied a constant potential difference across the graphite surface. During voltage measurements, the negative probe of the multimeter was fixed to the negative terminal of the battery and defined as 0 V (ground), while the positive probe was moved along the graphite starting at the 0 m position and then at measured intervals.

Two configurations were tested as shown in Fig. 1B: a uniform 0.05 m by 0.01 m graphite region with no defects, and a 0.05 m by 0.01 m graphite region containing a 0.01 m by 0.005 m centered gap, therefore making two 0.0025 m bridges on either side.

B. Voltage measurements

A digital multimeter (Fluke 106; Everett, WA) was used to measure voltage and resistance. During voltage measurements, the negative probe was fixed to the negative electrode, serving as a reference ground, while the positive probe was placed at various locations along the conductive region. Connections are as shown in Fig. 1B.

All voltage measurements for both the uniform and the defect configuration were taken along the centerline of the graphite surface (0.0025 m vertically). Voltage measurements were taken by moving the test lead at known distances from the reference electrode from left to right: 0.01 m, 0.02 m, 0.025 m, 0.03 m, 0.04 m, 0.05 m. The same measurement positions were used for both the uniform surface and the surface containing a defect to allow for direct comparison.

For the defect configuration at the gap where no conductive material was present, a direct centerline measurement could not be taken. Instead, measurements were taken at the edges of the gap on both sides, and this value was used to represent the voltage at that position. No measurements were taken off the centerline for any other points.

TABLE I
VOLTAGE MEASUREMENTS ALONG THE CENTERLINE FOR UNIFORM SURFACE.

distance, cm	predicted voltage, V	measured voltage, V
0.0	0.0	0.00
1.0	1.8	1.69
2.0	2.9	2.84
2.5	4.5	4.62
3.0	5.4	5.26
4.0	7.2	7.12
5.0	9.0	8.98

Data and analysis code for plots using R [19], [20] are available at https://github.com/devangel77b/426ccanada-lab10.

III. Results

Fig. 2 and Tables I and II show the voltage measurements for the uniform surface and the defect surface.

IV. Discussion

A. Utility in detecting a flaw

For the uniform surface, the measured voltages matched a linear distribution, as expected from (1) and (2). The defect surface deviated from the linear distribution. Since the voltages had noticeable discrepancies at corresponding locations between the uniform block and the non-uniform block (Fig. 2),

TABLE II
VOLTAGE MEASUREMENTS ALONG THE CENTERLINE FOR THE DEFECT SURFACE.

distance, cm	measured voltage, V	region
0.0	0.00	electrode
1.0	0.31	intact
2.0	0.42	start of gap
2.5	3.51	mid-gap
3.0	8.30	end of gap
4.0	8.59	intact
5.0	9.00	electrode

we successfully showed a non-destructive testing method using measurements of electric voltage to reveal defects in conductive materials.

B. What the heck does this mean?

A larger surface area for the graphite would have provided both advantages. A larger, wider conductor has a greater cross-sectional area, resulting in a lower resistance. However, depending on how well the conductor is made, a larger amount of imperfection is also likely due to the greater amount of error possible on a larger surface, further decreasing the resistance than within a smaller, more controlled area. Additionally, there are also discrepancies involving the paper clips supplying the graphite surface with current: only the tips of the paper clips were in contact with the graphite; had they been in more contact, the electric potential would be easily measured and more accurate.

ACKNOWLEDGEMENT

TA, MA, CC, DJ, AL, and TN worked equally on the experiments and writeup. We thank the Manalapan High School Science & Engineering program for support. We also thank several anonymous peer reviewers for helpful comments.

REFERENCES

[1] J. R. Davis, *Non-Destructive Evaluation of Materials*. Materials Park, OH: ASM International, 2004.
[2] P. Cawley, "Non-destructive testing—current capabilities and future directions," *Proceedings of the Institution of Mechanical Engineers, Part L: Journal of Materials: Design and Applications*, vol. 215, pp. 213–223, 2001.
[3] M. H. Loke, J. E. Chambers, D. F. Rucker, O. Kuras, and P. B. Wilkinson, "Recent developments in the direct-current geoelectrical imaging method," *Journal of Applied Geophysics*, vol. 95, pp. 135–156, 2013.
[4] A. Hauptmann, M. Ikehata, H. Itou, and S. Siltanen, "Revealing cracks inside conductive bodies by electric surface measurements," *Inverse Problems*, vol. 35, p. 025004, 2018.
[5] S. Ayyagari, V. Collemi, K. Shah, and K. Tomazic, "Computational mapping analysis of equipotential and electric field lines in gel electrophoresis rig," *Journal of Science & Engineering*, vol. 1, pp. 37–40, 2024.
[6] S. Baru, V. Choudhary, P. Thaker, N. Martin, and D. Ahmad, "Demonstrating a method to create a low-cost electrophoresis rig solution," *Journal of Science & Engineering*, vol. 1, pp. 42–44, 2024.
[7] R. Cohen, S. Musuku, J. Hammer, E. Handique, N. Patel, D. Gandhi, and N. Gershteyn, "Visualizing electric potential: mapping equipotential lines in a conductive water tray," *Journal of Science & Engineering*, vol. 1, pp. 45–47, 2024.
[8] R. Edwards, C. Karabin, C. Li, K. Patel, and J. Schatz, "Electric field mapping for cost-effective gel electrophoresis applications," *Journal of Science & Engineering*, vol. 1, pp. 49–52, 2024.
[9] A. Kumar, S. Perkins, N. Muthukumar, H. Villaseñor, and A. Khanna, "Mapping electric potential and electric field distribution in saltwater and investigating the effect of distance from source," *Journal of Science & Engineering*, vol. 1, pp. 53–55, 2024.
[10] National Institute of Standards and Technology (NIST), "Electrical conductivity of graphite materials," https://webbook.nist.gov/cgi/cbook.cgi?ID=C7782425, 2026, accessed: Mar 2026.
[11] D. J. Griffiths, *Introduction to Electrodynamics*, 4th ed. Boston, MA: Pearson Education, 2013.
[12] C. Kittel, *Introduction to Solid State Physics*, 8th ed. Hoboken, NJ: Wiley, 2004.
[13] C. R. Nave, "Doing it by the numbers: Javascript calculations in web-based instructional material," in *AAPT Summer Meeting*, Guelph, Ontario, 2000, http://hyperphysics.phy-astr.gsu.edu/hbase/electric/equipot.html.
[14] P. A. Tipler and G. Mosca, *Physics for Scientists and Engineers*, 5th ed. New York: W H Freeman and Company, 2004.
[15] R. A. Pelcovits and J. Farkas, *Barron's AP Physics C Premium*. Fort Lauderdale, FL: Kaplan North America, 2024.
[16] W. Moebs, S. J. Ling, and J. Sanny, *University Physics*. Houston, TX: OpenStax, 2016, vol. 1.
[17] R. D. Knight, *Physics for Scientists and Engineers: a strategic approach*, 4th ed. Pearson, 2017.
[18] J. D. Jackson, *Classical Electrodynamics*, 3rd ed. John Wiley & Sons, 1999.
[19] R Core Team, *R: A Language and Environment for Statistical Computing*, R Foundation for Statistical Computing, Vienna, Austria, 2025. [Online]. Available: https://www.R-project.org/
[20] H. Wickham, *ggplot2: Elegant Graphics for Data Analysis*. Springer-Verlag New York, 2016. [Online]. Available: https://ggplot2.tidyverse.org

Tushaar Akula is a senior in the Science and Engineering Magnet Program at Manalapan High School. He is president of the Astronomy Club and the Rocketry Club and competes in the American Rocketry Challenge. He enjoys wrestling, anime, and sidereal time, and plans to present an interpretive dance of Mars sidereal time before graduation.

Miguel Arenas is a senior in the Science and Engineering Magnet Program at Manalapan High School. When he is not studying multivariate calculus, he is an avid tennis player. He enjoys telling spoilers, especially of the Pickle Rick episode of Rick and Morty. He was an intern at Commvault in Tinton Falls, NJ and is currently doing a study of tennis biomechanics.

Cole Canada is a senior in the Science and Engineering Magnet Program at Manalapan High School. He is president of the Astronomy Club and enjoys swimming, volunteering, and sidereal time. He is an Eagle Scout and is passionate about niche anime. He was recently inducted into the National Honor Society.

Daivik Jajoo is a senior in the Science and Engineering Magnet Program at Manalapan High School. He was a civil engineering intern at Waterman LLC and is currently developing an augmented reality laser tag game.

Anton Lavrenov is a senior in the Science and Engineering Magnet Program at Manalapan High School. He is currently an intern at Matrix New World Engineering. When he is not studying multivariate calculus, he enjoys Drama Club, band, and the design and construction of full-scale medieval siege weaponry.

Timur Neyir is a senior in the Science and Engineering Magnet Program at Manalapan High School. He is currently doing a study of tennis biomechanics and the other students make fun of his tennis serve. He does not enjoy jumping.

Numerical simulation of electrical non-destructive testing of metals for flaw detection via the finite difference method

Jophy Lin, Sagarika Yagnyeshwaran, Rishith Chandra Kilaru, Srilekha Dantu, and Vijita Ayyangar

***Abstract*—The detection of internal flaws in a 3D-printed metal sample was simulated using a non-destructive testing (NDT) approach on a 2D grid. A finite difference method on a square grid of size 60 × 60 nodes was used to compute the electric potential across the material, and Successive Over-Relaxation (SOR) was applied to efficiently solve the linear equations. By iterating over the finite difference grid and updating the electric potential at each point until a set tolerance was reached, changes in voltage across the material became apparent. Regions with significant positive and negative voltage deviations indicated the presence and location of a crack near the center of the domain of the conductivity map. This method matters because it demonstrates how computational techniques can be used to detect defects in metal components without physically damaging them, which is useful in manufacturing and materials inspection.**

***Index Terms*—computational, 3D printing, Gauss-Seidel, finite difference, Python, conductivity, Laplace's equation, Poisson's equation, finite difference method, successive over-relaxation**

I. Introduction

3D PRINTING conductive materials, including metals and conductive polymers, allows for complex designs and rapid production, but can introduce internal defects. These include cracks and incomplete bonding between layers. These flaws may significantly degrade mechanical strength or electrical performance while remaining invisible to external inspection [1].

Common non-destructive testing (NDT) techniques, such as x-ray imaging or ultrasonic inspection, often require specialized equipment or a multitude of expenditures that may not be available in testing environments [2], [3]. As a result, simpler and more accessible methods for defect detection are in demand.

Electrical probing provides a potential alternative, as internal changes in conductivity could alter current paths and voltage distributions [4]. Because voltage can be measured at the surface of a metal, internal defects may be detected indirectly through imperfections in the observed voltage field.

Previous researchers examined voltage mapping to experimentally characterize the equipotentials and electric fields within a low-cost gel electrophoresis device [5]–[9]. However, this previous work did not attempt numerical simulation.

Author for correspondence: 126jlin@frhsd.com

Authors are with the Science & Engineering Magnet Program, Manalapan High School, 20 Church Lane, Englishtown, NJ 07726, USA

10.64804/z4c41213

In this work, the feasibility of electrical non-destructive testing is investigated using a finite-difference computational model of steady-state conduction [10]. By comparing voltage distributions in a uniform conductive sheet to those obtained in the presence of an internal low-conductivity defect, localized voltage perturbations are identified. These deviations from the baseline voltage field indicate the presence and approximate location of internal flaws.

The following is the hypothesis being tested in this experiment: if there is no flaw, there should be no measurable change in voltage:

$$H_0 : \Delta V = V_{flaw} - V_{clean} = 0 \tag{1}$$

In the case that the flaw exists, the voltage distribution changes, showing a measurable disruption in the surface of the material. This can be modeled by the following equation:

$$H_1 : \Delta V = V_{flaw} - V_{clean} \neq 0 \tag{2}$$

II. Methods and materials

Under steady-state conditions and in the absence of internal current, electrical conduction in a material with varying conductivity $\sigma(x, y)$ is governed by

$$\vec{\nabla} \cdot (\sigma \vec{\nabla} V) = 0 \tag{3}$$

where $V(x, y)$ is the electric potential. The material was assumed to be isotropic, and time-dependent factors were neglected.

The conductive domain was modeled as a two-dimensional square region on a regular uniform $60 \times 60\,\mathrm{node}$ finite-difference grid. This was to ensure that each node was relatively small compared to the simulated piece of metal, similar to how a real piece of metal has near-infinitely small particles. All voltages were evaluated at the grid nodes, with uniform spacing between each node for simplicity.

Fixed-potential (Dirichlet) boundary conditions were applied on the left and right boundaries of the domain, with voltages of $1.0\,\mathrm{V}$ and $0.0\,\mathrm{V}$, respectively, representing the source and sink electrodes. The top and bottom boundaries were treated as electrically insulating by enforcing zero normal voltage gradients. Together, these boundaries establish a controlled voltage field across the metal, allowing the low-conductivity regions to locally distort the voltage field.

To simulate defects in the metal, we modeled localized regions of lower electrical conductivity. Because a flawless piece

of metal that has no defects would be uniformly conductive, the lower conductivity represents the absence of metal, which is the gaps and cracks in a real piece of metal. The conductivity of the flawless material was set constant to 1.0, while the conductivity of the flawed regions was set constant to 1×10^{-9}, both in normalized units.

The governing equation was discretized using a finite-difference formulation that enforces current conservation at each grid node. Conductivity at cell interfaces was computed using the harmonic mean to accurately represent sharp conductivity contrasts. The harmonic mean was used because it models how current flows across materials with varying conductivities. Current is slowed down by the poorly conductive region, which is the crack, and so by taking the harmonic mean, the weight is shifted towards the smaller value. This method allows us to ensure that the current is conserved and prevents the overestimation of conductivity at the boundaries by clearly showing the defect.

Since we needed to find the voltage at all 3600 points, we would either use the Jacobi method or the Gauss-Seidel [10] method to solve the resulting system of linear equations. The Gauss-Seidel method updates the nodes individually based on the neighboring nodes, whereas the Jacobi method updates all nodes simultaneously using values from the previous iteration, making the Jacobi method computationally expensive. This is why the Gauss-Seidel method was implemented, where each calculation uses updated information rather than waiting for an entire iteration through the grid; the formula below was used to update the voltage of each node:

$$V_{i,j}^{(\mathrm{GS})} = \frac{\sigma_{i+\frac{1}{2},j}\,V_{i+1,j} + \sigma_{i-\frac{1}{2},j}\,V_{i-1,j} + \sigma_{i,j+\frac{1}{2}}\,V_{i,j+1} + \sigma_{i,j-\frac{1}{2}}}{\sigma_{i+\frac{1}{2},j} + \sigma_{i-\frac{1}{2},j} + \sigma_{i,j+\frac{1}{2}} + \sigma_{i,j-\frac{1}{2}}} \tag{4}$$

Successive-Over-Relaxation [10] (SOR) is the process of iteratively solving systems of linear equations by accelerating the convergence of the Gauss-Seidel Method. In order to further optimize and increase the speed of the program, we used the Successive-Over-Relaxation (SOR) technique until the maximum change in voltage between iterations fell below 1×10^{-6} V using the below formula:

$$V_{i,j}^{(n+1)} = (1-\omega)V_{i,j}^{(n)} + \omega V_{i,j}^{(\mathrm{GS})} \tag{5}$$

The electric field was computed from the converged voltage distribution using:

$$\vec{E} = -\vec{\nabla}V \tag{6}$$

To isolate the perturbations induced by the defects, the voltage difference field was calculated as such:

$$\Delta V = V_{flaw} - V_{clean} \tag{7}$$

The voltage difference field was then analyzed as the primary non-destructive testing signal. Numerical computations were performed in Python using the `numpy` and `matplotlib` libraries [11], [12]. A Jupyter notebook [13] with finite difference code is available at https://github.com/usernnamee/NDT-Testing-SOR and https://jupyter.snerds.org. Data and code are also available at https://github.com/devangel77b/427syagnyeshwaran-lab3.

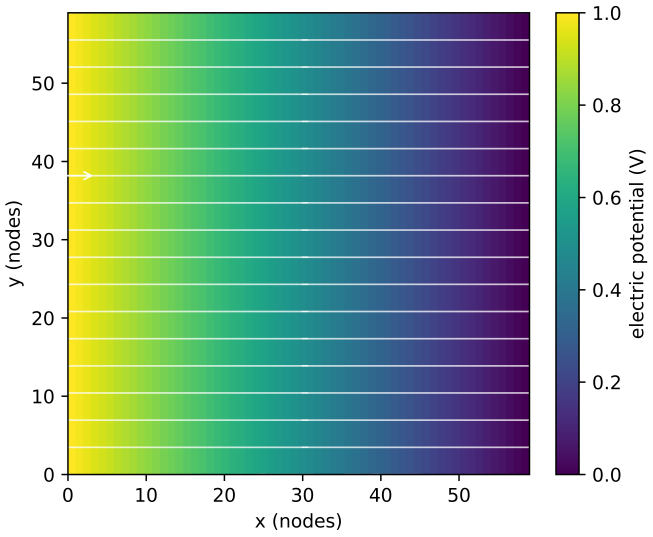

Fig. 1. Electric potential distribution for a uniform conductive sheet with no internal flaw.

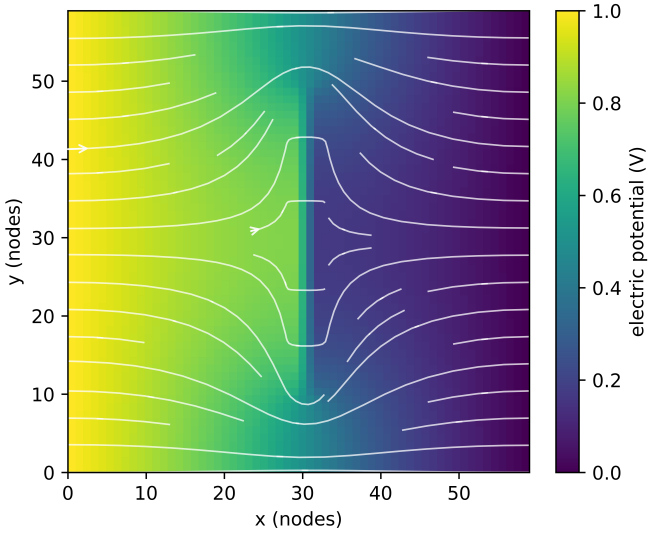

Fig. 2. Electric potential distribution for a conductive sheet containing a low-conductivity flaw.

III. Results

The electric potential is shown in Fig. 1 for a uniform 3D-printed metal with no internal flaw present.

The potential distribution after adding a flaw is shown in Fig. 2, with arrows representing the potential field lines that outline the shape of the flaw and defect. In this simulation, the flaw is a thin, vertical crack.

Fig. 3 shows the voltage difference, evidently highlighting the location at which there is an internal flaw. The blue voltage difference represents a location at which the voltage drops and the current is rerouted, whereas the red voltage difference represents a location at which the voltage is higher than expected, and the current is being impeded upstream.

The shape of the flaw inserted into the surface of the metallic material is depicted in Fig. 4.

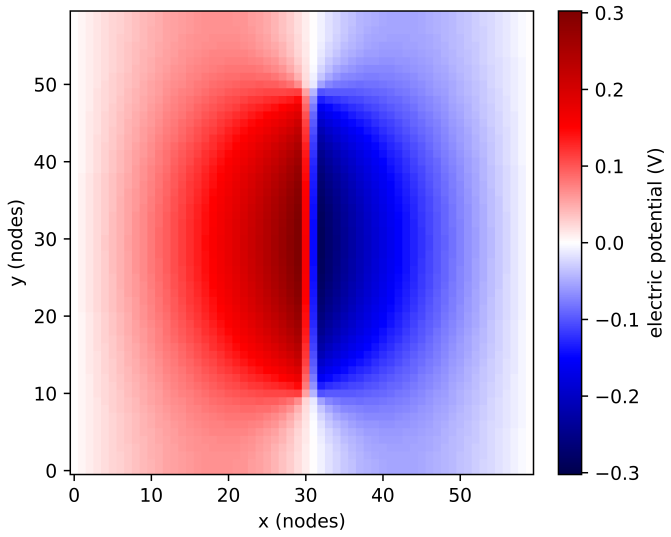

Fig. 3. Voltage difference (ΔV) between the defect-free and defective cases, serving as the electrical NDT signal.

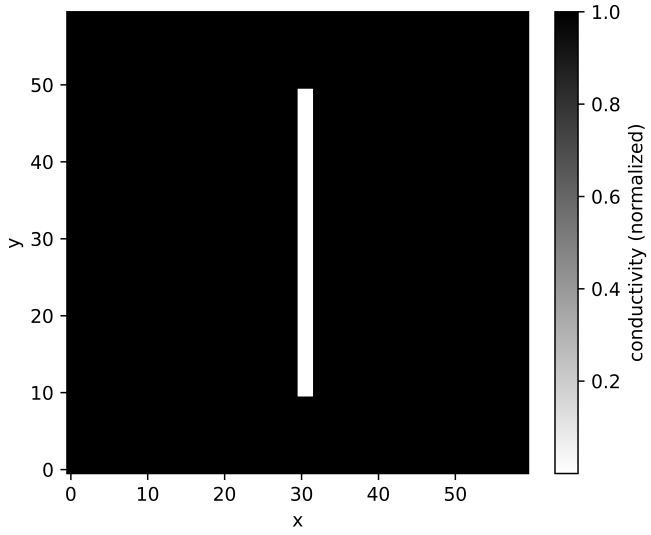

Fig. 4. Conductivity map of the simulated conductive sheet showing the location and geometry of the introduced flaw.

These results support the idea that electrical probing is a viable non-destructive testing method for conductive 3D-printed materials, as changes in voltage reflect hidden disruptions in conductivity without physically damaging the part to test for imperfections.

IV. Discussion

The behavior observed in this study can be explained by how electric current responds to changes in conductivity within a material.

In a conductive sheet with no defects, current distributes evenly and the voltage changes smoothly across the surface. When a flaw is present, the local conductivity is reduced, which increases resistance and forces current to reroute around the damaged region.

This rerouting causes uneven voltage changes that can be detected at the surface, even though the defect itself is internal. Because voltage depends directly on how current flows through the material, small disruptions in conductivity can produce noticeable differences in the measured potential.

Therefore, we reject the null hypothesis; flaws resulting in observable voltage differences than can be used as a diagnostic tool, subject to some conditions. This study is limited by the use of a simplified two-dimensional model and idealized material properties, which do not capture all aspects of real 3D-printed metal parts. Similarly, when using grids of different resolutions (30 by 30 and 120 by 120 in other tests), while keeping the size of the flaw relative to the grid constant, there was very little change in the observed pattern. The maximum voltage difference remained constant across different grid resolutions, which confirms grid convergence as it is independent of grid size. The spatial resolution and conductivity difference between the base material and the flaw will effect the minimum size of flaw that can be detected.

In practice, defects may have complex shapes, varying depths, and partial conductivity rather than being fully insulating. Future work could extend this approach to three-dimensional models, explore different defect sizes and conductivities, and experiment with various kinds of metals. Experimental validation using physical conductive materials or 3D-printed samples would further test the practicality of this method for real-world NDT applications.

In the future, we aim to make this process more precise by detecting the absence or presence of a flaw by testing the outer boundaries rather than interior. This is more accurate to real life since in a practical NDT situation, we only have access to the surface and not the interiors

Appendix

The following Python code was used to implement the finite-difference solver, apply boundary conditions, compute the electrical field, and generate Figs. 1 to 4. The code makes use of the `numpy` and `matplotlib` libraries [11], [12]. Relaxation or Gauss-Seidel is implemented around line 59, while successive over-relaxation is implemented around line 62 [10].

```
1  import numpy as np
2  import matplotlib.pyplot as plt
3
4  Nx, Ny = 60, 60
5  iters = 8000
6  tol = 1e-6
7
8  def harmonic_mean(a, b, eps=1e-12):
9      return (2.0 * a * b) / (a + b + eps)
10
11 def compute_electric_field(V, hx=1.0, hy=1.0):
12     dVdi, dVdj = np.gradient(V, hx, hy, edge_order=2)
13     Ex = -dVdj
14     Ey = -dVdi
15     return Ex, Ey
16
17 def solve_fd_conductance(with_flaw=False, omega=1.8):
18     sigma = np.ones((Nx, Ny), dtype=float)
19     if with_flaw:
20         sigma[10:50, 30:32] = 1e-9
21
22     V = np.zeros((Nx, Ny), dtype=float)
23     for j in range(Ny):
24         V[:, j] = 1.0 + (0.0 - 1.0) * (j / (Ny - 1))
25
```

```
    fixed = np.zeros((Nx, Ny), dtype=bool)
    fixed[:, 0] = True
    fixed[:, -1] = True

    def apply_bc(V):
        V[:, 0] = 1.0
        V[:, -1] = 0.0
        V[0, :] = V[1, :]
        V[-1, :] = V[-2, :]

    apply_bc(V)

    for _ in range(iters):
        max_delta = 0.0
        for i in range(1, Nx - 1):
            for j in range(1, Ny - 1):
                if fixed[i, j]:
                    continue

                ip, im = i + 1, i - 1
                jp, jm = j + 1, j - 1

                sxp = harmonic_mean(sigma[i, j], sigma[ip, j])
                sxm = harmonic_mean(sigma[i, j], sigma[im, j])
                syp = harmonic_mean(sigma[i, j], sigma[i, jp])
                sym = harmonic_mean(sigma[i, j], sigma[i, jm])

                A = sxp + sxm + syp + sym
                if A < 1e-20:
                    continue

                # The next line implements relaxation or
                # lazy Gauss-Seidel
                V_ideal = (sxp * V[ip, j] + sxm * V[im, j] +
                           syp * V[i, jp] + sym * V[i, jm]) / A

                # The next line implements successive over-relaxation
                V_old = V[i, j]
                V[i, j] = (1.0 - omega) * V_old + omega * V_ideal

                delta = abs(V[i, j] - V_old)
                if delta > max_delta:
                    max_delta = delta

        apply_bc(V)
        if max_delta < tol:
            break

    return V, sigma

def add_arrowheads(ax, stream, color="white", lw=1.0):
    segs = stream.lines.get_segments()
    if len(segs) == 0:
        return

    k = 12
    for idx in range(0, len(segs), k):
        seg = segs[idx]
        (x0, y0), (x1, y1) = seg[0], seg[1]
        ax.annotate(
            "",
            xy=(x1, y1),
            xytext=(x0, y0),
            arrowprops=dict(arrowstyle="->", color=color,
                            linewidth=lw, shrinkA=0,
                            shrinkB=0),
        )

# Run
V_clean, sigma_clean = solve_fd_conductance(with_flaw=False)
V_flaw, sigma_flaw = solve_fd_conductance(with_flaw=True)

V_diff = V_flaw - V_clean

Ex_clean, Ey_clean = compute_electric_field(V_clean)
Ex_flaw, Ey_flaw = compute_electric_field(V_flaw)

# PLOTTING (four figures)

x = np.arange(Nx)
y = np.arange(Ny)
X, Y = np.meshgrid(x, y)

# No flaw (V + E streamlines)
fig,ax = plt.subplots(figsize=(5,4), constrained_layout=True, dpi=1200)
im0 = ax.imshow(V_clean, origin="lower", cmap="viridis", vmin=0, vmax=1, extent=[0,Nx-1,0,Ny-1])
s0 = ax.streamplot(
    X, Y, Ex_clean, Ey_clean,
    density=0.6,
    linewidth=0.9,
    color=(1, 1, 1, 0.75),
    arrowstyle='-'
)
add_arrowheads(ax, s0, color=(1, 1, 1, 0.9), lw=1.0)
ax.set_xlabel("x (nodes)")
ax.set_ylabel("y (nodes)")
cb0=plt.colorbar(im0, ax=ax)
cb0.set_label("electric potential (V)")
fig.savefig("potential-noflaw.png",dpi=1200)
plt.close(fig)

# With flaw (V + E streamlines)
fig,ax = plt.subplots(figsize=(5,4), constrained_layout=True, dpi=1200)
im1 = ax.imshow(V_flaw, origin="lower", cmap="viridis", vmin=0, vmax=1,extent=[0,Nx-1,0,Ny-1])
s1 = ax.streamplot(
    X, Y, Ex_flaw, Ey_flaw,
    density=0.6,
    linewidth=0.9,
    color=(1, 1, 1, 0.75),
    arrowstyle='-'
)

add_arrowheads(ax, s1, color=(1, 1, 1, 0.9), lw=1.0)
ax.set_xlabel("x (nodes)")
ax.set_ylabel("y (nodes)")
cb1=plt.colorbar(im1, ax=ax)
cb1.set_label("electric potential (V)")
fig.savefig("potential-flaw.png",dpi=1200)
plt.close(fig)

# Difference signal
fig,ax = plt.subplots(figsize=(5,4), constrained_layout=True, dpi=1200)
dvmax = np.max(np.abs(V_diff))
im2 = ax.imshow(V_diff, origin="lower", cmap="seismic", vmin=-dvmax, vmax=dvmax)
ax.set_xlabel("x (nodes)")
ax.set_ylabel("y (nodes)")
cb2=plt.colorbar(im2, ax=ax)
cb2.set_label("electric potential (V)")
fig.savefig("potential-difference.png",dpi=1200)
plt.close(fig)

# Conductivity map
fig,ax = plt.subplots(figsize=(5,4), constrained_layout=True, dpi=1200)
im3 = ax.imshow(sigma_flaw, origin="lower", cmap="gray_r")
ax.set_xlabel("x")
ax.set_ylabel("y")
cb3=plt.colorbar(im3, ax=ax)
cb3.set_label("conductivity (normalized)")
fig.savefig("conductivity.png",dpi=1200)
plt.close(fig)
```

ACKNOWLEDGEMENT

The team thanks all group members for their collaborative contributions to this work, including code development, simulation design, and manuscript writing. This work was made possible through close teamwork and collaboration among all group members throughout the research and writing process.

Additionally, the team acknowledges the Science and Engineering Magnet Program for providing access to the Jupyter Notebook computing environment used to develop, run, and test the simulations. Lastly, the team would like to thank all peers who have provided constructive feedback and review, helping improve the quality of this work.

REFERENCES

[1] N. Dalal, Y. Gu, D. R. Hines, A. Dasgupta, and S. Das, "Cracks in the 3d-printed conductive traces of silver nanoparticle ink," *Journal of Micromechanics and Microengineering*, vol. 29, p. 097001, 2019.

[2] P. Cawley, "Non-destructive testing—current capabilities and future directions," *Proceedings of the Institution of Mechanical Engineers, Part L: Journal of Materials: Design and Applications*, vol. 215, pp. 213–223, 2001.

[3] J. R. Davis, *Non-Destructive Evaluation of Materials*. Materials Park, OH: ASM International, 2004.

[4] A. Hauptmann, M. Ikehata, H. Itou, and S. Siltanen, "Revealing cracks inside conductive bodies by electric surface measurements," *Inverse Problems*, vol. 35, p. 025004, 2018.

[5] S. Ayyagari, V. Collemi, K. Shah, and K. Tomazic, "Computational mapping analysis of equipotential and electric field lines in gel electrophoresis rig," *Journal of Science & Engineering*, vol. 1, pp. 37–40, 2024.

[6] S. Baru, V. Choudhary, P. Thaker, N. Martin, and D. Ahmad, "Demonstrating a method to create a low-cost electrophoresis rig solution," *Journal of Science & Engineering*, vol. 1, pp. 42–44, 2024.

[7] R. Cohen, S. Musuku, J. Hammer, E. Handique, N. Patel, D. Gandhi, and N. Gershteyn, "Visualizing electric potential: mapping equipotential lines in a conductive water tray," *Journal of Science & Engineering*, vol. 1, pp. 45–47, 2024.

[8] R. Edwards, C. Karabin, C. Li, K. Patel, and J. Schatz, "Electric field mapping for cost-effective gel electrophoresis applications," *Journal of Science & Engineering*, vol. 1, pp. 49–52, 2024.

[9] A. Kumar, S. Perkins, N. Muthukumar, H. Villaseñor, and A. Khanna, "Mapping electric potential and electric field distribution in saltwater and investigating the effect of distance from source," *Journal of Science & Engineering*, vol. 1, pp. 53–55, 2024.

[10] W. H. Press, S. A. Teukolsky, W. T. Vetterling, and B. P. Flannery, *Numerical Recipes in C: the art of scientific computing*, 2nd ed. Cambridge University Press, 1992.

[11] C. R. Harris, K. J. Millman, S. J. van der Walt, R. Gommers, P. Virtanen, D. Cournapeau, E. Wieser, J. Taylor, S. Berg, N. J. Smith, R. Kern, M. Picus, S. Hoyer, M. H. van Kerkwijk, M. Brett, A. Haldane, J. F. del Río, M. Wiebe, P. Peterson, P. Gérard-Marchant, K. Sheppard, T. Reddy, W. Weckesser, H. Abbasi, C. Gohlke, and T. E. Oliphant, "Array programming with NumPy," *Nature*, vol. 585, pp. 357–362, 2020.

[12] J. D. Hunter, "Matplotlib: A 2d graphics environment," *Computing in Science & Engineering*, vol. 9, pp. 90–95, 2007.

[13] T. Kluyver, B. Ragan-Kelley, F. Pérez, B. Granger, M. Bussonnier, J. Frederic, K. Kelley, J. Hamrick, J. Grout, S. Corlay, P. Ivanov, D. Avila, S. Abdalla, and C. Willing, "Jupyter Notebooks – a publishing format for reproducible computational workflows," in *Positioning and Power in Academic Publishing: Players, Agents and Agendas*, F. Loizides and B. Schmidt, Eds. IOS Press, 2016, pp. 87–90.

Jophy Lin is a senior in the Science and Engineering Magnet Program at Manalapan High School. She was also a member of Hackathon Leadership Team. She is a member of the Research Club and enjoys labubus, hanging out in Harvard Square, projective geometry, RNA folding, and streaming foreign language dramas.

Sagarika Yagnyeshwaran is a senior in the Science and Engineering Magnet Program at Manalapan High School. She was also an intern at Commvault in Tinton Falls, NJ. She enjoys heads up displays, Trivia Club, Hackathon Leadership Team, concert chorus, and streaming foreign language dramas.

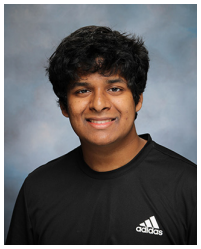

Rishith Chandra Kilaru is a senior in the Science and Engineering Magnet Program at Manalapan High School. He was also an intern at WIT Sports in New York, and a member of Hackathon Leadership Team. When he is not building augmented reality video games, he enjoys karaoke, ramen, and writing, and is famous for BONELAB modding.

Srilekha Dantu is a senior in the Science and Engineering Magnet Program at Manalapan High School. She enjoys working on AP Physics C E&M and on senior projects such as a low-cost intravenous weight monitoring device and a Spiderman grapple gun.

Vijita Ayyangar is a senior in the Science and Engineering Magnet Program at Manalapan High School. She is an intern at I-House Architecture in Belmar, NJ and a member of the Drama Club. In her free time, she enjoys working on AP Physics C E&M.

Index of Authors